Nano Research 2014, 7(8): 1232–1240
DOI 10.1007/s12274-014-0486-z
Research Article
ISSN 1998-0124
CN 11-5974/O4

High thermal conductivity of suspended few-layer hexagonal boron nitride sheets

Haiqing Zhou[1,2], Jixin Zhu[3,4], Zheng Liu[4], Zheng Yan[1], Xiujun Fan[1,5], Jian Lin[3,6], Gunuk Wang[1], Qingyu Yan[4] (✉), Ting Yu[2] (✉), Pulickel M. Ajayan[3,6] (✉), and James M. Tour[1,3,6] (✉)

[1] *Department of Chemistry, Rice University, 6100 Main Street, Houston, Texas 77005, USA*
[2] *Division of Physics and Applied Physics, School of Physical and Mathematical Sciences, Nanyang Technological University, 637371, Singapore*
[3] *Department of Materials Science and NanoEngineering, Rice University, 6100 Main Street, Houston, Texas 77005, USA*
[4] *School of Materials Science and Engineering, Nanyang Technological University, Nanyang Avenue, 639798, Singapore*
[5] *College of Electronic Information and Control Engineering, Beijing University of Technology, Beijing, 100124, China*
[6] *The Smalley Institute for Nanoscale Science and Technology, Rice University, 6100 Main Street, Houston, Texas 77005, USA*

Received: 10 March 2014
Revised: 23 April 2014
Accepted: 24 April 2014

KEYWORDS
two-dimensional,
hexagonal boron nitride (h-BN),
thermal conductivity,
Raman spectroscopy

ABSTRACT

The thermal conduction of suspended few-layer hexagonal boron nitride (h-BN) sheets was experimentally investigated using a noncontact micro-Raman spectroscopy method. The first-order temperature coefficients for monolayer (1L), bilayer (2L) and nine-layer (9L) h-BN sheets were measured to be $-(3.41 \pm 0.12) \times 10^{-2}$, $-(3.15 \pm 0.14) \times 10^{-2}$ and $-(3.78 \pm 0.16) \times 10^{-2}$ $cm^{-1} \cdot K^{-1}$, respectively. The room-temperature thermal conductivity of few-layer h-BN sheets was found to be in the range from 227 to 280 $W \cdot m^{-1} \cdot K^{-1}$, which is comparable to that of bulk h-BN, indicating their potential use as important components to solve heat dissipation problems in thermal management configurations.

1 Introduction

Hexagonal boron nitride (h-BN) is a common nontoxic material used for its low electrical conductivity, high thermal conductivity, and superior lubricant properties. Analogous to graphene, h-BN is a two-dimensional (2D) honeycomb-structured crystal, in which an equal number of alternating B and N atoms are covalently bonded with sp^2 hybridization and yet demonstrate remarkable ionic character [1–3]. Recently, h-BN has been found to be an important 2D crystal and dielectric gate substrate for graphene because the atomically smooth surface and strong bonding of h-BN significantly improves carrier mobilities in

Address correspondence to James M. Tour, tour@rice.edu; Pulickel M. Ajayan, ajayan@rice.edu; Ting Yu, yuting@ntu.edu.sg; Qingyu Yan, alexyan@ntu.edu.sg

graphene by a factor of 10 when compared to those of graphene on SiO_2 [3–5]. Furthermore, compared to SiO_2, h-BN is an appealing dielectric substrate for graphene devices because its atomically smooth surface is relatively free of dangling bonds and charge traps, which leads to weak electronic interlayer coupling between graphene and h-BN sheets, and thus preserves the electronic and optical properties intrinsic to graphene [3–6]. Due to its geometric similarity, h-BN possesses some physical properties similar to graphene, such as strong mechanical properties [7, 8] and high chemical and thermal stability [7, 9–11]. Given that the strong bonding of atoms such as C–C and B–N results in a large phonon contribution, as exemplified in BN, carbon nanotubes and graphene, it is expected that the h-BN crystal could have a high thermal conductivity [12–15]. However, recent research on h-BN mainly focuses on its large-scale synthesis [16–20] and optical and electronic properties [1–3, 5, 21, 22] rather than the thermal properties [23]. Therefore, motivated by the superior thermal conductivity of graphene, it is imperative to determine whether h-BN sheets also possess high thermal conductivity, thus better understanding its properties as a component in electrical and thermal management devices.

With the decrease in feature sizes of microelectronic devices and circuits, the dissipation power density significantly increases. Consequently, efficient heat removal or conduction becomes a crucial design characteristic for next-generation integrated circuits, electronic and optoelectronic devices, in which thermal conduction is a key limiting factor to further device miniaturization. It is known that traditional Si-based semiconductors show a dramatic suppression of thermal conductivity at the nanometer scale, while insulators such as Si_3N_4, SiO_2, and Al_2O_3 used in microelectronic devices are all poor thermal conductors in their usual forms. But for bulk h-BN, it is interesting to note that its thermal conductivity is ~390 $W \cdot m^{-1} \cdot K^{-1}$, which is 280 times larger than that of SiO_2. For thin h-BN sheets, the thermal conductivity value could exceed, or be comparable to, that of its bulk crystalline form [14, 15]. In addition, because layered h-BN is an electrical insulator with a wide band-gap (5.5–6.0 eV), chemical inertness and possibly good thermal conductivity, integrating h-BN with graphene has become a common approach to experimental device fabrication. Hence it is desirable to find a suitable, simple method to evaluate the thermal conductivity of thin h-BN sheets. The synthesis of large-scale and highly crystalline h-BN sheets with controlled layers via low pressure chemical vapor deposition (LPCVD) has been demonstrated [8, 24–26], thereby providing an opportunity to explore the thermal conductivity of h-BN sheets.

In the present work, using confocal micro-Raman spectroscopy, a nondestructive and unconventional approach for the noncontact measurement of the thermal conductivity of suspended h-BN sheets synthesized by a LPCVD method was demonstrated. The Raman spectra of monolayer (1L), bilayer (2L) and 9-layer (9L) h-BN sheets were found to be dependent on the surrounding temperature, and the peak frequencies of the Raman E_{2g} mode vary linearly with temperature. The first-order temperature coefficients of the Raman E_{2g} mode for these samples were: $-(3.41 \pm 0.12) \times 10^{-2}$, $-(3.15 \pm 0.14) \times 10^{-2}$ and $-(3.78 \pm 0.16) \times 10^{-2}$ $cm^{-1} \cdot K^{-1}$, respectively. The thermal conductivity of suspended 9L h-BN sheets at room temperature was around 243 $W \cdot m^{-1} \cdot K^{-1}$, which is comparable to that of bulk h-BN, indicating its potential use in components for heat dissipation in thermal management, especially when the 9L h-BN serves as a dielectric gate substrate for graphene/h-BN integrated nanodevices.

2 Experimental

For the growth of h-BN [26], 12.5 μm thick Ni foils (Goodfellow, Inc. Purity: 99.9%) were placed in the centre of a tube furnace and gradually heated to 950 ℃ over 40 min and was then annealed at 950 ℃ for 10 min in 500 sccm Ar/H_2 gas flow (15 vol% H_2 balanced by 85 vol% Ar) with a chamber pressure ~800 mTorr. Subsequently, the furnace was gradually heated to 1,000 ℃ in 10 min. Ammonia borane (NH_3–BH_3) was sublimed at 130 ℃ using a heating element and the gas was carried into the reaction zone by the Ar/H_2 carrier gas. During the growth process, the total flow of mixed Ar/H_2 gas (15 vol% H_2 balanced by 85 vol% Ar) was kept at 300 sccm with a pressure ~400 mTorr and the thickness of h-BN was controlled by changing the growth time (7 min for 1L, 10 min for

2L and 20 min for 9L). After the growth, the furnace was quickly cooled to room temperature. As reported in our previous work [8, 24–26], the as-grown h-BN films on Ni foils were removed from the furnace, and spin-coated with a thin film of poly(methyl methacrylate) (PMMA, MicroChem Corp. 950 PMMA A4, 4% in anisole) atop. The underlying Ni substrate was dissolved in a dilute nitric acid solution. Then the films were transferred to other substrates for further characterization after the removal of the thin PMMA film by soaking in acetone for 30 min.

The micro-Raman spectroscopy (Renishaw inVia Raman Spectroscope) experiments were carried out under ambient conditions using 514.5 nm laser excitation with a laser spot size ~1 μm. During the measurements of temperature-dependent Raman spectra, the laser power was set below 0.5 mW so as to avoid local laser heating on samples. Many Raman spectra (~10) of h-BN sheets were collected to ensure the credibility and repeatability of the results.

3 Results and discussion

The h-BN sheets used here were grown on 12.5 μm thick nickel foils using a previously reported LPCVD method [8, 24–26]. We transferred the as-grown samples onto the 150 nm Au film-coated silicon substrate with many pre-patterned trenches for measuring thermal conductivity. The details are shown in the Electronic Supplementary Material (ESM). Some of the h-BN films were transferred onto silicon substrates for further characterization. Before thermal transport measurements, the uniformity and quality of the h-BN samples were examined by optical microscopy (OM), Raman spectroscopy, scanning electron microscopy (SEM), atomic force microscopy (AFM) and X-ray photoelectron spectroscopy (XPS) as shown in Fig. 1 and Figs. S1 and S2 (in the ESM). In order to differentiate the transferred h-BN film from the silicon substrate, a trench was scratched using tweezers, marked by a white arrow in Fig. 1(a). As is indicated in the optical image (Fig. 1(a)), the h-BN film is mainly 2L, as confirmed by the AFM (Fig. S1 in the ESM) and subsequent TEM characterization. The typical height of the h-BN film was ~1 nm as indicated in the inset of Fig. S1 (in the ESM). There are some areas that are marked by blue arrows, which appear to be 1L h-BN sheet (Fig. 1(a)). The color contrast between these thin regions and the silicon substrate is nearly undetectable [19]. However, an obvious Raman signal with a Raman peak located at 1,370 cm^{-1} (corresponding to the E_{2g} vibration mode of h-BN) can be identified in the regions marked by blue arrows, indicating it is from 1L h-BN. The Raman spectra of layered materials are sensitive to their quality and film thickness. In order to correlate the Raman signal to the thickness of the h-BN, we have recorded the Raman spectra from different thicknesses of the CVD-grown h-BN sheets that have been placed on silicon substrates with a 285-nm-thick SiO_2 layer (Fig. 1(b)). It was found that the peak intensities of the Raman E_{2g} mode at ~1,370 cm^{-1} are strongly related to the h-BN thickness and increase with an increase in layer number. In addition, the peak position of bulk h-BN shifts toward lower frequency compared to 1L, 2L and thin h-BN sheets (~9 layers as determined by TEM characterization, vide infra). These Raman signatures are consistent with those reported for mechanically exfoliated h-BN sheets [27], indicating the high quality and crystallinity of the samples.

XPS characterization was performed to determine the composition and stoichiometric ratio of B:N. The XPS spectra are shown in Figs. 1(c) and 1(d), from which it can be determined that a B1s-core level is present at 190.1 eV (marked in Fig. 1(c)), which is nearly identical to that previously reported for bulk boron nitride with a hexagonal phase [28, 29]. The N1s peak is located at 397.7 eV (Fig. 1(d)) very close to the reported position of the N1s spectrum (398.1 eV) of h-BN [28, 29]. The stoichiometric ratio of B:N atoms in the h-BN samples was calculated to be ~1.10 based on an XPS survey. The slightly higher nitrogen may come from residual nitric acid used for the transfer process.

Transmission electron microscopy (TEM) was performed to characterize the microscopic structures of the h-BN sheets. Figures 2(a) and 2(b) are high-resolution TEM images of 1L and 2L h-BN sheets, respectively. These TEM images further support the suggestion of 1L and 2L h-BN sheets in Fig. 1(a).

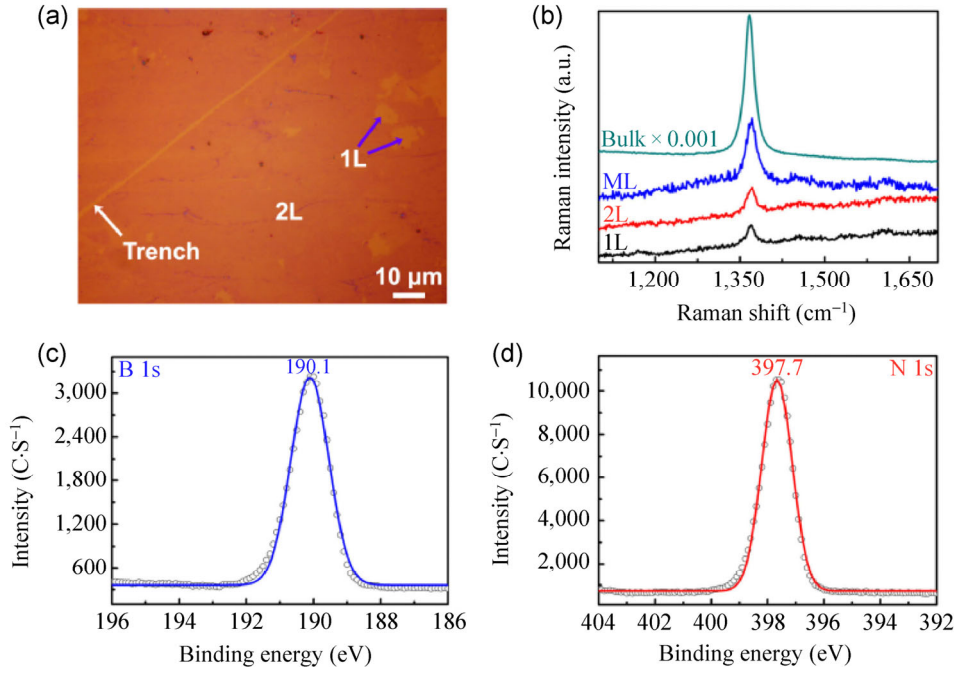

Figure 1 (a) An optical image of 1L and 2L h-BN sheets on a SiO_2/Si substrate containing a trench. (b) Raman spectra of n-layer h-BN sheets on a SiO_2/Si substrate. XPS spectra of an h-BN film on the silicon substrate; (c) B1s spectrum and (d) N1s spectrum.

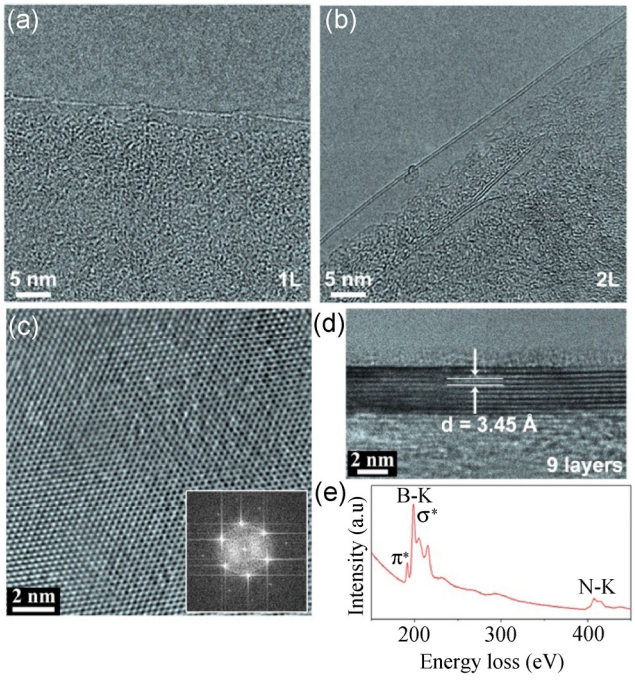

Figure 2 TEM characterization of h-BN films with different thicknesses. (a) High-magnification TEM showing the edge of a 1L h-BN sheet. (b) HRTEM showing the edge of a 2L h-BN sheet. (c) HRTEM image showing hexagonal atomic arrays as well as its corresponding FFT pattern (shown in the inset) on the h-BN surface, indicating the high crystallinity and quality of the as-grown h-BN samples. (d) HRTEM showing the edge of the investigated h-BN film, which is 9L, based on the number of lines at the folding edge. (e) A typical EELS spectra collected on a thin h-BN film.

Figure 2(c) shows a high-resolution TEM (HRTEM) image taken from the surface of a few-layer h-BN sheet. The hexagonal lattice can be seen in this image. The corresponding six-fold-symmetry fast Fourier transform (FFT, inset in Fig. 2(c)) pattern confirms the hexagonal structure and multiple layers of h-BN. These results suggest the highly crystalline nature of the h-BN sheet. In its cross-sectional TEM image, shown in Fig. 2(d), this thin h-BN sheet has ~9 atomic layers as determined by the number of lines at the folding edge. The interlayer distance of the h-BN film is ~3.45 Å, which is similar to that of bulk h-BN. The electron energy loss spectrum (EELS) is shown in Fig. 2(e). There are two visible edges starting at ~180 and 390 eV, which can be attributed to the characteristic K-shell ionization edges of B and N, respectively [30, 31]. In addition, the presence of the characteristic π* and σ* energy loss peaks at the boron K edge suggests sp^2-hybridized bonding and a hexagonal structure consisting of B and N in the h-BN samples [30], which is consistent with HRTEM observation of the surface (Fig. 2(c)). The TEM analyses of the h-BN film confirm the single crystal nature of the examined areas and high quality of the as-grown thin h-BN films.

As recently reported, there are two Raman spectroscopic parameters that can be used to evaluate the thermal conductivity of two-dimensional layered materials such as graphene [32–34] and thin MoS_2 flakes [35]. The first is the first-order temperature coefficient in the Raman scattering of the investigated samples, which can be directly extracted from temperature-dependent Raman spectra and the almost linear relationship between Raman peak frequencies and the surrounding temperature. This coefficient can be obtained by measuring the corresponding Raman spectra of silicon-supported samples with the substrate temperature controlled by an external heating stage (see the ESM). Figure 3 shows the temperature-dependent Raman spectra of 1L, 2L and 9L h-BN sheets with the substrate temperature ranging from 298 to 448 K. To ensure the credibility and repeatability of the temperature-dependent Raman data, the relevant Raman spectra were collected as the substrate temperatures were cooled (Fig. S3, in the ESM). As shown in Figs. 3(a), 3(c), and 3(e), the Raman E_{2g} modes red-shifts for 1L, 2L and 9L h-BN flakes are detected, which are sensitive to the surrounding temperature due to the B–N bond strength change. As the temperature increased from 313 to 433 K, red Raman shifts of E_{2g} mode were 4.0, 4.1, and 4.4 cm^{-1} for 1L, 2L and 9L h-BN sheets, respectively. Correspondingly, when the temperature decreased from 433 to 313 K, blue Raman shifts of E_{2g} modes were observed that were 4.3, 3.7, and 4.1 cm^{-1} for 1L, 2L and 9L h-BN sheets, respectively. These Raman shifts of the E_{2g} mode for different increases

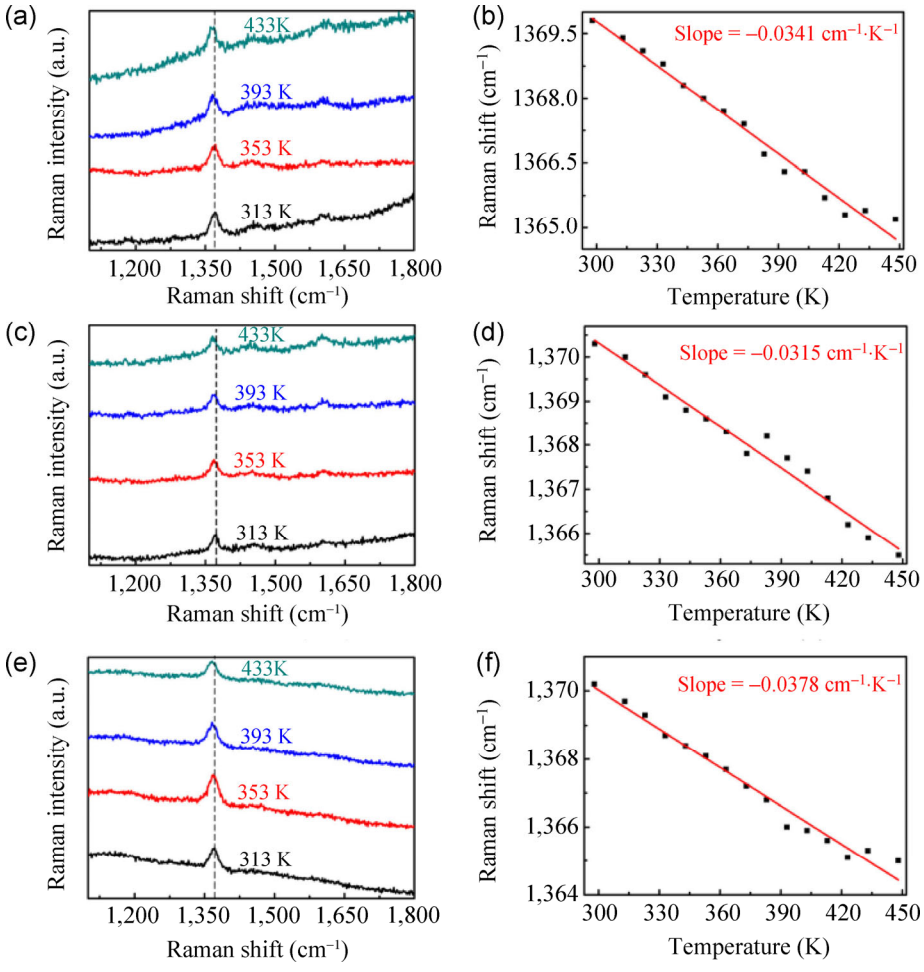

Figure 3 Heating temperature-dependent Raman spectra of 1L, 2L and 9L h-BN sheets. Raman frequency evolution in the Raman scattering of (a) 1L, (c) 2L and (e) 9L h-BN sheets at four temperatures. The frequencies for the Raman E_{2g} mode in the Raman scattering of (b) 1L, (d) 2L and (f) 9L h-BN sheets, respectively, as a function of temperature, ranging from room temperature to 448 K. The data were fitted using linear functions, as shown by the red lines.

and decreases in h-BN flake temperature are quite similar. In addition, the peak frequency temperature variation for the E_{2g} modes could be fitted using linear functions, which are shown in Figs. 3(b), 3(d), and 3(f) with solid straight lines for 1L, 2L and 9L h-BN sheets, respectively. These results suggest the strong dependence of the E_{2g} mode on the surrounding temperature. In view of similar temperature-dependent Raman behaviors in graphene, the temperature dependence of the E_{2g} mode frequency shift in h-BN sheets can be described by Eq. (1)

$$\omega(T) = \omega_0 + \chi \times T \quad (1)$$

where ω_0 is the frequency of the E_{2g} mode when the absolute temperature T is extrapolated to 0 K and χ is the first-order temperature coefficient. Based on the slopes of the fitted straight lines in Figs. 3(b), 3(d), and 3(f), the relevant first-order temperature coefficients of the E_{2g} modes for 1L, 2L and 9L h-BN sheets can be extrapolated and are $-(3.41 \pm 0.12) \times 10^{-2}$, $-(3.15 \pm 0.14) \times 10^{-2}$, and $-(3.78 \pm 0.16) \times 10^{-2}$ $cm^{-1} \cdot K^{-1}$, respectively.

The other main parameter for the thermal conductivity measurement of h-BN is the dependence of the Raman E_{2g} mode frequency on the excitation laser power.

A schematic diagram of the thermal conductivity measurements by Raman spectroscopy is shown in Fig. 4(a). To measure the thermal conductivity intrinsic to h-BN flakes by Raman spectroscopy, the samples need to be suspended so as to avoid rapid heat dissipation to the silicon substrate. The silicon substrates were prepared by photolithography and dry etching of Si substrates covered with a 300 nm SiO_2 layer. Prior to the sample transfer, a 150 nm gold film, which served as the heat sink, was thermally deposited onto the silicon substrate with regular trench arrays. Each trench was a rectangle with a length of 40 μm, a width of 7 μm and a depth of nearly 300 nm (Fig. S4 in the ESM). Figures 4(b) and 4(c) present the typical optical and SEM images of the h-BN film suspended over the trenches, respectively. From these images, we can find that the h-BN film covers the entire trench area with some production of wrinkles in the film. To ensure that the trench was fully covered by the h-BN film, Raman spectra were collected at different positions across an individual trench. The variation of Raman frequency shifts with the laser power was investigated in detail by tuning the external laser power.

Since the size of the trench is much larger than the spatial resolution of the laser spot (~1 μm), the laser

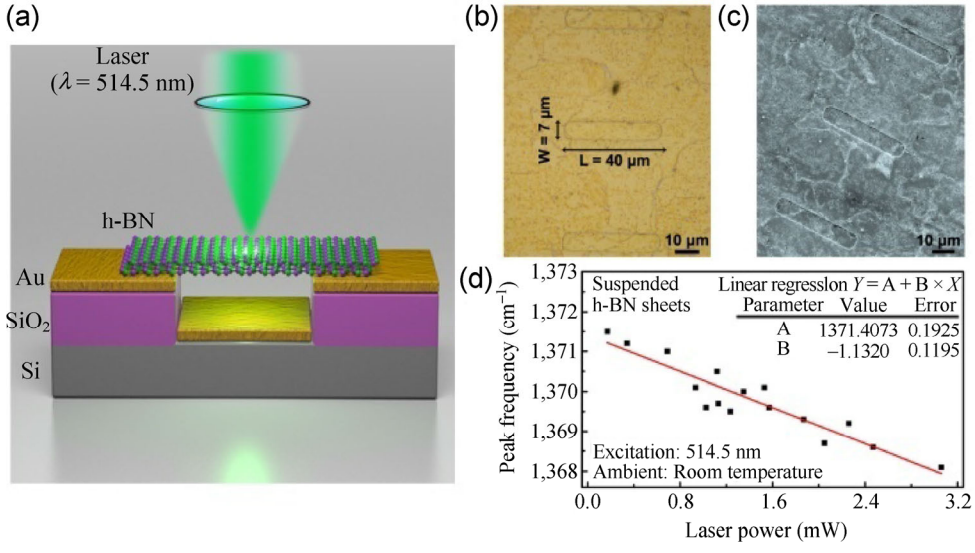

Figure 4 (a) A schematic diagram showing the excitation laser light focused on an h-BN film suspended across a trench. The typical (b) optical and (c) SEM images of a suspended h-BN film(~9L). (d) Laser power-dependent peak frequency of Raman E_{2g} mode in a suspended h-BN film.

can be easily focused in the middle region of the suspended h-BN sheets. Due to the almost negligible thermal conduction of air (~0.025 $W \cdot m^{-1} \cdot K^{-1}$), the convection losses of laser power to the air for our geometric design are relatively low (0.86 μW). When an external laser is irradiated on the sample surface, the laser energy is partially absorbed (Fig. S5, in the ESM), resulting in heat generation in the suspended h-BN that propagates through the extremely thin h-BN film. The laser heating should produce an obvious temperature rise in the central region, which would then be detected on the basis of Raman frequency shifts, as the E_{2g} mode is very sensitive to external heating (Fig. 3). The deposited gold film in the trench edge serves as a heat sink such that the temperature is somewhat unchanged when a laser irradiates the sample with low power level. Therefore, the heat generated by the laser irradiation should propagate toward the heat sink.

The heat conduction across any material surface with the areas can be expressed by Eq. (2)

$$\frac{\partial Q}{\partial t} = -\mathrm{K}\oint \nabla T \cdot \mathrm{d}\vec{s} \quad (2)$$

where Q is the amount of heat transferred 2D layered materials such as graphene. Given that the radial heat flow propagates from the middle of the suspended flake toward the trench edges, similar to that in few-layer MoS_2 [35], the expression for the thermal conductivity of thin h-BN sheets is evaluated in Eq. (3)

$$K = \chi\left(\frac{1}{2\pi h}\right)\left(\frac{\delta\omega}{\delta P}\right)^{-1}\left(\frac{\delta P_{\text{h-BN}}}{\delta P}\right) \quad (3)$$

where χ is the first-order temperature coefficient extracted in Fig. 3, h is the thickness of the h-BN film, ω is the peak frequency shift of Raman E_{2g} mode, $P_{\text{h-BN}}$ is the absorbed laser power by the suspended h-BN film, and P is the external laser power. Using Raman spectroscopy, we have measured the variation of the Raman E_{2g} mode frequency with the external laser power for a number of suspended samples over the trenches. The excitation power over the sample surface was measured with a power meter. Figure 4(d) presents the frequency shifts of the E_{2g} mode as a function of the incident laser power for a 9L h-BN film, rather than 1L and 2L h-BN sheets. This is because it is still difficult to detect any Raman signals originating from 1L and 2L h-BN sheets when they are suspended over the holes. As shown in Fig. 4(d), it is evident that, as the laser power increases, the E_{2g} mode frequency shifts toward lower frequency due to the local laser heating. Considering that the Raman shift is less than 3.4 cm^{-1}, which corresponds to a temperature rise of ~90 K in the central region of the sheet, the relationship between Raman frequency shift and external laser power can be described by a linear function, from which we can extract the value of the term from Eq. (3), namely $\delta\omega/\delta P = -1.13\ cm^{-1} \cdot mW^{-1}$. As a result, on the basis of the following parameters: h = 3.0 nm, $\delta P_{\text{h-BN}}/\delta P$ = 10% (see the ESM, Part 5, noting that the transmitted light through the h-BN would be mainly reflected from the gold/silicon at the bottom of the trench), the thermal conductivity of 9L h-BN sheets was calculated to be in the range from 227 to 280 $W \cdot m^{-1} \cdot K^{-1}$. This value is comparable to that of bulk h-BN, and close to that of 5L h-BN measured by built-in resistance thermometers [23]. This is due to the interlayer coupling in multilayer h-BN, which results in the breaking of the phonon scattering selection rule in 1L h-BN, thus reducing the relevant thermal conductivity values. The values converge to that of bulk h-BN when the layer thickness is increased to five layers or more [14, 36, 37]. The value of the thermal conductivity is also comparable to that of boron nitride nanotubes reported previously [13]. Even though the thermal conductivity of few-layer h-BN sheets has been well-documented by theoretical calculations [14, 15], experimental confirmation has been lacking until now. Consequently, this finding will be useful in enlarging the applications of h-BN sheets as important components in thermal management.

4 Conclusions

In conclusion, we report the experimental investigation of thermal conduction in suspended few-layer h-BN sheets using a noncontact confocal micro-Raman spectroscopy technique. The room-temperature thermal conductivity of few-layer h-BN sheets was measured to be ~243 $W \cdot m^{-1} \cdot K^{-1}$, which suggests that h-BN sheets can outperform silicon oxides as a gate dielectric material with excellent heat conduction.

Meanwhile, this study should enlarge the range of h-BN applications as the thermal management material of choice in optoelectronics, photonics, and electronics, and pave the way for efficient thermal management in two-dimensional layered materials.

Acknowledgements

Dr. Haiqing Zhou and Dr. Jixin Zhu contributed equally to this work. This project was supported by the Singapore National Research Foundation under NRF RF Award No. NRF-RF2010-07, the AFOSR MURI (FA9550-12-1-0035), Air Force Office of Scientific Research (FA9550-09-1-0581), U.S. Army Research Office MURI grant W911NF-11-1-0362 and the U.S. Office of Naval Research MURI grant N000014-09-1-1066.

Electronic Supplementary Material: This material is available in the online version of this article at http://dx.doi.org/10.1007/s12274-014-0486-z.

References

[1] Kubota,Y.; Watanabe, K.; Tsuda, O.; Taniguchi, T. Deep ultraviolet light-emitting hexagonal boron nitride synthesized at atmospheric pressure. *Science* **2007**, *317*, 932–934.

[2] Alem, N.; Erni, R.; Kisielowski, C.; Rossell, M. D.; Gannett, W.; Zettl, A. Atomically thin hexagonal boron nitride probed by ultrahigh-resolution transmission electron microscopy. *Phys. Rev. B* **2009**, *80*, 155425.

[3] Gannett, W.; Regan, W.; Watanabe, K.; Taniguchi, T.; Crommie, M. F.; Zettl, A. Boron nitride substrates for high mobility chemical vapor deposited grapheme. *Appl. Phys. Lett.* **2011**, *98*, 242105.

[4] Dean, C. R.; Young, A. F.; Meric, I.; Lee, C.; Wang, L.; Sorgenfrei, S.; Watanabe, K.; Taniguchi, T.; Kim, P.; Shepard, K. L. et al. Boron nitride substrates for high-quality graphene electronics. *Nat. Nanotechnol.* **2010**, *5*, 722–726.

[5] Watanabe, K.; Taniguchi, T.; Kanda, H. Direct-bandgap properties and evidence for ultraviolet lasing of hexagonal boron nitride single crystal. *Nat. Mater.* **2004**, *3*, 404–409.

[6] Wang, M.; Jang, S. K.; Jang, W. J.; Kim, M.; Park, S. Y.; Kim, S. W.; Kahng, S. J.; Choi, J. Y.; Ruoff, R. S.; Song, Y. J. et al. A platform for large-scale graphene electronics – CVD growth of single-layer graphene on CVD-grown hexagonal boron nitride. *Adv. Mater.* **2013**, *25*, 2746–2752.

[7] Zhi, C. Y.; Bando, Y.; Tang, C. C.; Kuwahara, H.; Golberg, D. Large-scale fabrication of boron nitride nanosheets and their utilization in polymeric composites with improved thermal and mechanical properties. *Adv. Mater.* **2009**, *21*, 2889–2893.

[8] Song, L.; Ci, L. J.; Lu, H.; Sorokin, P. B.; Jin, C. H.; Ni, J.; Kvashnin, A. G.; Kvashnin, D. G.; Lou, J.; Yakobson, B. I. et al. Large scale growth and characterization of atomic hexagonal boron nitride layers. *Nano Lett.* **2010**, *10*, 3209–3215.

[9] Lipp, A.; Schwetz, K. A.; Hunold, K. Hexagonal boron nitride: Fabrication, properties and applications. *J. Eur. Ceram. Soc.* **1989**, *5*, 3–9.

[10] Kho, J. G.; Moon, K. T.; Kim, J. H.; Kim, D. P. Properties of boron nitride (B_xN_y) films produced by the spin-coating process of polyborazine. *J. Am. Ceram. Soc.* **2000**, *83*, 2681–2683.

[11] Chen, Y.; Zou, J.; Campbell, S. J.; Caer, G. L. Boron nitride nanotubes: Pronounced resistance to oxidation. *Appl. Phys. Lett.* **2004**, *84*, 2430.

[12] Chang, C. W.; Han, W. Q.; Zettl, A. Thermal conductivity of B–C–N and BN nanotubes. *Appl. Phys. Lett.* **2005**, *86*, 173102.

[13] Chang, C. W.; Fennimore, A. M.; Afanasiev, A.; Okawa, D.; Ikuno, T.; Garcia, H.; Li, D. Y.; Majumdar, A.; Zettl, A. Isotope effect on the thermal conductivity of boron nitride nanotubes. *Phys. Rev. Lett.* **2006**, *97*, 085901.

[14] Lindsay, L.; Broido, D. A. Theory of thermal transport in multilayer hexagonal boron nitride and nanotubes. *Phys. Rev. B* **2012**, *85*, 035436.

[15] Ouyang, T.; Chen, Y. P.; Xie, Y.; Yang, K. K.; Bao, Z. G.; Zhong, J. X. Thermal transport in hexagonal boron nitride nanoribbons. *Nanotechnology* **2010**, *21*, 245701.

[16] Shi, Y. M.; Hamsen, C.; Jia, X. T.; Kim, K. K.; Reina, A.; Hofmann, M.; Hsu, A. L.; Zhang, K.; Li, H. N.; Juang, Z. Y. et al. Synthesis of few-layer hexagonal boron nitride thin film by chemical vapor deposition. *Nano Lett.* **2010**, *10*, 4134–4139.

[17] Kim, K. K.; Hsu, A.; Jia, X. T.; Kim, S. M.; Shi, Y. M.; Hofmann, M.; Nezich, D.; Rodriguez-Nieva, J. F.; Dresselhaus, M. S.; Palacios, T. et al. Synthesis of monolayer hexagonal boron nitride on Cu foil using chemical vapor deposition. *Nano Lett.* **2012**, *12*, 161–166.

[18] Lee, K. H.; Shin, H. J.; Lee, J.; Lee, I.; Kim, G. H.; Choi, J. Y.; Kim, S. W. Large-scale synthesis of high-quality hexagonal boron nitride nanosheets for large-area graphene electronics. *Nano Lett.* **2012**, *12*, 714–718.

[19] Kim, K. K.; Hsu, A.; Jia, X. T.; Kim, S. M.; Shi, Y. M.; Dresselhaus, M.; Palacios, T.; Kong, J. Synthesis and characterization of hexagonal boron nitride film as a dielectric layer for graphene devices. *ACS Nano* **2012**, *6*, 8583–8590.

[20] Kim, G.; Jang, A. R.; Jeong, H. Y.; Lee, Z.; Kang, D. J.; Shin, H. S. Growth of high-crystalline, single-layer hexagonal boron nitride on recyclable platinum foil. *Nano Lett.* **2013**, *13*, 1834–1839.

[21] Kubota, Y.; Watanabe, K.; Tsuda, O.; Taniguchi, T. Deep ultraviolet light-emitting hexagonal boron nitride synthesized at atmospheric pressure. *Science* **2007**, *317*, 932–934.

[22] Levendorf, M. P.; Kim, C. J.; Brown, L.; Huang, P. Y.; Havener, R. W.; Muller, D. A.; Park, J. Graphene and boron nitride lateral heterostructures for atomically thin circuitry. *Nature* **2012**, *488*, 627–632.

[23] Jo, I.; Pettes, M. T.; Kim, J.; Watanabe, K.; Taniguchi, T.; Yao, Z.; Shi, L. Thermal conductivity and phonon transport in suspended few-layer hexagonal boron nitride. *Nano Lett.* **2013**, *13*, 550–554.

[24] Liu, Z.; Song, L.; Zhao, S. Z.; Huang, J. Q.; Ma, L. L.; Zhang, J. N.; Lou, J.; Ajayan, P. M. Direct growth of graphene/hexagonal boron nitride stacked layers. *Nano Lett.* **2011**, *11*, 2032–2037.

[25] Ci, L. J.; Song, L.; Jin, C. H.; Jariwala, D.; Wu, D. X.; Li, Y. J.; Srivastava, A.; Wang, Z. F.; Storr, K.; Balicas, L. et al. Atomic layers of hybridized boron nitride and graphene domains. *Nat. Mater.* **2010**, *9*, 430–435.

[26] Liu, Z.; Ma, L. L.; Shi, G.; Zhou, W.; Gong,Y. J.; Lei, S. D.; Yang, X. B.; Zhang, J. N.; Yu, J. J.; Hackenberg, K. P. et al. In-plane heterostructures of graphene and hexagonal boron nitride with controlled domain sizes. *Nat. Nanotechnol.* **2013**, *8*, 119–124.

[27] Gorbachev, R. V.; Riaz, I.; Nair, R. R.; Jalil, R.; Britnell, L.; Belle, B. D.; Hill, E. W.; Novoselov, K. S.; Watanabe,K.; Taniguchi, T. et al. Hunting for monolayer boron nitride: Optical and raman signatures. *Small* **2011**, *7*, 465–468.

[28] Park, K. S.; Lee, D. Y.; Kim, K. J.; Moon, D. W. Observation of a hexagonal BN surface layer on the cubic BN film grown by dual ion beam sputter deposition. *Appl. Phys. Lett.* **1997**, *70*, 315.

[29] Lee, K. S.; Kim, Y. S.; Tosa, M.; Kasahara, A.; Yosihara, K. Mechanical properties of hexagonal boron nitride synthesized from film of Cu/BN mixture by surface segregation. *Appl. Surf. Sci.* **2001**, *169–170*, 420–424.

[30] Chopra, N. G.; Luyken, R. J.; Cherrey, K.; Crespi, V. H.; Cohen, M. L.; Louie, S. G.; Zettl, A. Boron Nitride Nanotubes. *Science* **1995**, *269*, 966–967.

[31] Mayer, J. C.; Chuvilin, A.; Algara-Siller, G.; Biskupek, J.; Kaiser, U. Selective sputtering and atomic resolution imaging of atomically thin boron nitride membranes. *Nano Lett.* **2009**, *9*, 2683–2689.

[32] Balandin, A. A.; Ghosh, S.; Bao, W. Z.; Calizo, I.; Teweldebrhan, D.; Miao, F.; Lau, C. N. Superior thermal conductivity of single-layer graphene. *Nano Lett.* **2008**, *8*, 902–907.

[33] Lee, J. U.; Yoon, D.; Kim, H.; Lee, S. W.; Cheong, H. Thermal conductivity of suspended pristine graphene measured by Raman spectroscopy. *Phys. Rev. B* **2011**, *83*, 081419.

[34] Cai, W. W.; Moore, A. L.; Zhu, Y. W.; Li, X. S.; Chen, S. S.; Shi, L.; Ruoff, R. S. Thermal transport in suspended and supported monolayer graphene grown by chemical vapor deposition. *Nano Lett.* **2010**, *10*, 1645–1651.

[35] Sahoo, S.; Gaur, A. P. S.; Ahmadi, M.; Guinel, M. J. F.; Katiyar, R. S. Temperature dependent Raman studies and thermal conductivity of few layer MoS_2. *J Phys. Chem. C* **2013**, *117*, 9042–9047.

[36] Ghosh, S.; Bao, W. Z.; Nika, D. L.;Subrina, S.; Pokatilov, E. P.; Lau, C. N.; Balandin, A. A. Dimensional crossover of thermal transport in few-layer graphene materials. *Nat. Mater.* **2010**, *9*, 555–558.

[37] Lindsay, L.; Broido, D. A.; Mingo, N. Flexural phonons and thermal transport in multilayer graphene and graphite. *Phys. Rev. B* **2011**, *83*, 235428.